Suspension Jams in a Leaky Microfluidic Channel

J. S. Yodh,[1] V. Spandan,[2] and L. Mahadevan[1,2,3,*]

[1]*Department of Physics, Harvard University, Cambridge, Massachusetts 02138, USA*
[2]*John A. Paulson School of Engineering and Applied Sciences, Harvard University, Cambridge, Massachusetts 02138, USA*
[3]*Department of Organismic and Evolutionary Biology, Harvard University, Cambridge, Massachusetts 02138, USA*

Inspired by the jamming in leaky systems that arises in many physiological and industrial settings, we study the propagation of clogs in a leaky microfluidic channel. By driving a colloidal suspension through such a channel with a fluid-permeable wall adjoining a gutter, we follow the formation and propagation of jams and show that they move at a steady speed, in contrast with jams in channels that have impermeable walls. Furthermore, by varying the ratio of the resistance from the leaky wall and that of the gutter, we show that it is possible to control the shape of the propagating jam, which is typically wedge shaped. We complement our experiments with numerical simulations, where we implement an Euler-Lagrangian framework for the simultaneous evolution of both immersed colloidal particles and the carrier fluid. Finally, we show that the particle ordering in the clog can be tuned by adjusting the geometry of the leaky wall. Altogether, the leaky channel serves both as a filter and a shunt with the potential for a range of uses.

When large numbers of particles move in confined geometries, they have a propensity to clog or jam with consequences for a range of fields including physiology [1–4], material science and industry [5–14], and cellular, organismal, and pedestrian traffic [15,16]. Most studies of the dynamics of formation and propagation of clogs focus on channel-like geometries with impermeable walls, where jamming can occur under a wide range of conditions, e.g., [17,18]. In these devices, clog growth slows down in time, clog front shape remains on average flat and perpendicular to the channel, and clog nucleation is stochastic with catastrophic consequences for flow control. This raises a natural question: can one control the speed and the shape of a clog by varying the geometry of the channel?

One might imagine that the introduction of a leaky wall that separates a microfluidic channel from an adjoining gutter would allow for control of the clog speed and shape reproducibly. The leaky wall then serves to filter large objects but allows fluid and small objects to leak through it and flow into the gutter. If a clog forms in such a system, the combination of the leaky wall and gutter would shunt fluid and divert it from the clog even as the latter grows via the accumulation of particles. A related channel geometry, that of a pipe with porous walls, has been rigorously studied experimentally and theoretically as a fluid dynamics problem, but here we focus on clog propagation in these devices [19–21].

To instantiate this idea, we consider an experimental system that uses monodispersed density-matched colloidal suspensions with variable packing fractions driven through microfluidic devices by a gravity-driven constant pressure head ($\Delta P \simeq 400$ Pa) as shown in Fig. 1(a). All devices are prepared using standard soft lithographic techniques [22]. In all experiments, we fix the depth and the length of the channels at 50 μm and 2 cm, respectively, the particle radius at $r = 20$ μm, and the distance between the top and bottom edges of the leaky walls at $w = 450$ μm. The channel itself consists of an inner leaky membrane with feature spacing d separating the channel from a gutter of width ℓ_g. To nucleate a clog, we introduce a leaky backwall that captures all colloidal particles.

The clog growth dynamics are controlled by the far-field concentration of colloids, ϕ_∞ and the far-field average velocity of colloids, u_∞. These quantities are measured far from the clog front using standard techniques [23,24]. As particles flow down the channel, they pile against the porous inner walls to form a clog that propagates backwards with speed u_s and position $s(t)$ measured from the tip of the clog wedge. We track the clog using digital video microscopy (100 frames per second) as shown in Fig. 1(b). The clog forms a wedge that propagates at constant speed, in sharp contrast with an unsteady blunt clog [see the Supplemental Material [25], Figs. S1(a) and S1(b), and [8]].

To understand this shape, we refer to the schematic in Fig. 1(c) depicting particles moving from left to right forming a clog at $s(t)$ moving from right to left. As the fluid nears the clog, the leakiness of the wall and the presence of a gutter cause fluid and particles to develop a transverse flow velocity; the fluid moves through the leaky wall, while the particles are blocked by it. To get a quantitative sense of the fluid shunting, we fix a clog in space by first flowing colloids down the channel before switching to a suspension of 500 nm fluorescent particles (see the Supplemental Material [25], Video 2). In Fig. 1(d), a particle image
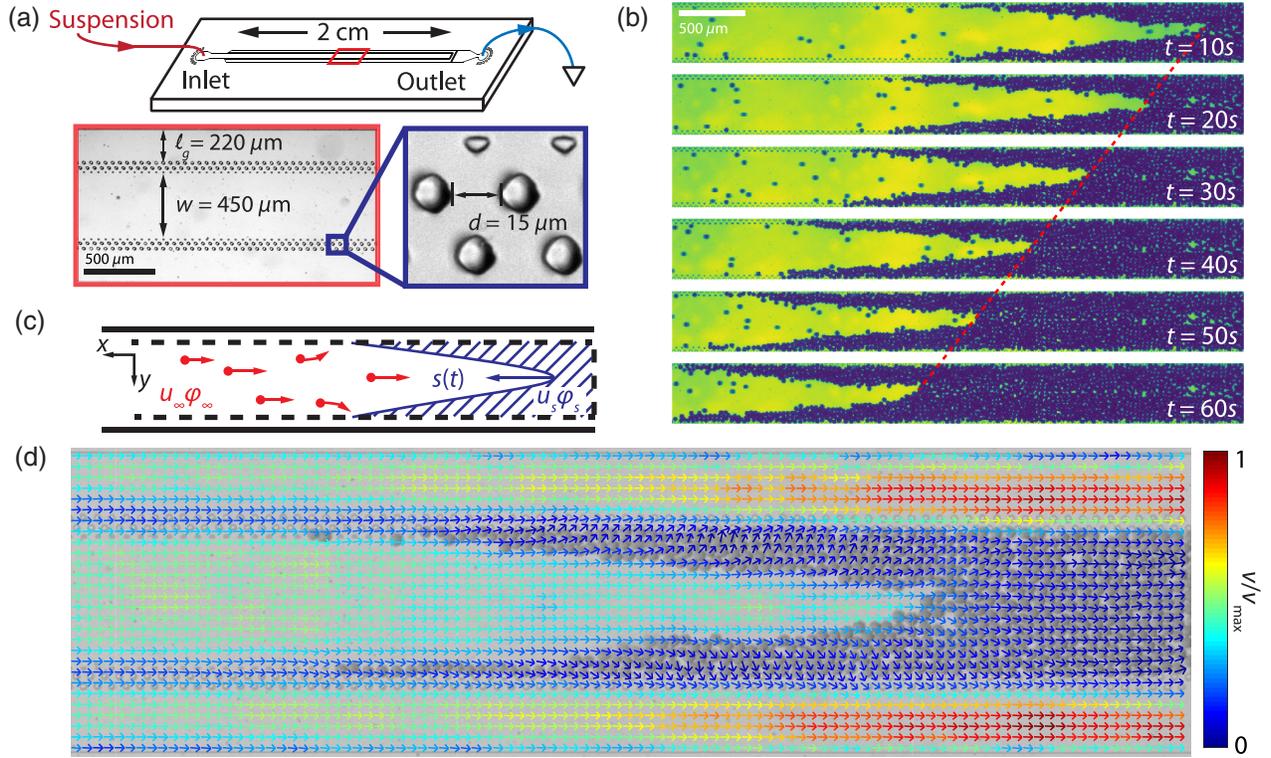
FIG. 1. (a) Top: schematic of experimental setup. A particle suspension driven by constant pressure head flows through a microfluidic channel with leaky walls and an adjoining gutter. Bottom: optical micrograph of the channel interior. The leaky inner wall is comprised of pillars spaced $d = 15$ μm apart. The channel has width, $w = 450$ μm, and the distance between the leaky membrane and the outer wall is $\ell_g = 220$ μm. (b) Time series of a clog propagating against the incident particles taken in 10-second intervals. The red dotted line indicates the clog front position. (c) Schematic of incident particles (red) with flux $u_\infty \phi_\infty$ forming a clog (blue) with flux $u_s \phi_s$. The position of the clog, $s(t)$, is measured from the tip of the clog wedge. Near the clogging front, incident particles can develop a component of velocity transverse to the channel. (d) PIV plot of the fluid velocity field (**v**) in the vicinity of a clog. The color bar is a linear scale normalized to the maximum fluid velocity ($v_{\max}$).

velocimetry (PIV) generated fluid velocity field [26], overlaid on a bright field image of a stationary clog, shows that while the fluid velocity to the left of the clog is largely uniform, as fluid approaches the clog, it is shunted to the gutters. Furthermore, in the interior of the clog, the fluid velocity decays towards zero rapidly.

To quantify the propagation dynamics of the clog, we measured $s(t)$ for devices with $d = 15$ μm and $\ell_g = 220$ μm. In Fig. 2(a) we show $s(t)$ for $\phi_\infty \in [3.7 \times 10^{-3}, 4.8 \times 10^{-2}]$ over 40 second windows. The slope of $s(t)$ is the measured clog propagation speed, $u_{s,m}$, which ranges between 102 μm/s at the highest incident packing fraction to 13.5 μm/s at the lowest incident packing fraction. Since $s(t)$ varies linearly with time for the duration of the experiment, the clog propagation speed is constant. We note that over longer timescales (hundreds of seconds), for this device geometry, we found that $s(t) \sim t^\gamma$, where $\gamma = 0.84$, due to increased hydraulic resistance in the channel [see the Supplemental Material [25], Fig. S1(c)]. Modeling the exponent γ, which depends on the ratio of w to ℓ_g, is an interesting problem in its own right. The shape of the clog is characterized by the angle θ^c (in radians)

between the advancing edge of the clogging front with the leaky membrane indicated in the top panel of Fig. 2(b). In the bottom panel of Fig. 2(b), $\theta^c(t)$ is plotted for different ϕ_∞ as a function of time. Though the angles fluctuate, the average angle remains fairly stable for the duration of the experiments indicating that the shape of the clog is fixed.

We can predict the clog propagation speed, $u_{s,p}$, using mass balance by balancing the flux of the incident particles, $u_\infty \phi_\infty$ with the flux due to the moving clogging front, $u_{s,p} \phi_s - u_{s,p} \phi_\infty$, so that

$$u_{s,p} = \frac{u_\infty \phi_\infty}{\phi_s - \phi_\infty}, \tag{1}$$

where the subscript p stands for predicted. To test this, we plot the normalized measured clog speeds, $\hat{u}_{s,m} = u_{s,m}/u_\infty$, against the normalized predicted clog speeds, $\hat{u}_{s,p} = u_{s,p}/u_\infty$ in Fig. 3(a) and see that $\hat{u}_{s,m} \simeq 0.5\hat{u}_{s,p}$. This discrepancy arises because we measure u_∞ far upstream of the clogging front instead of just to the left its advancing edge. Since particles slow down as they approach the clog, $u_{s,p}$ is overestimated.
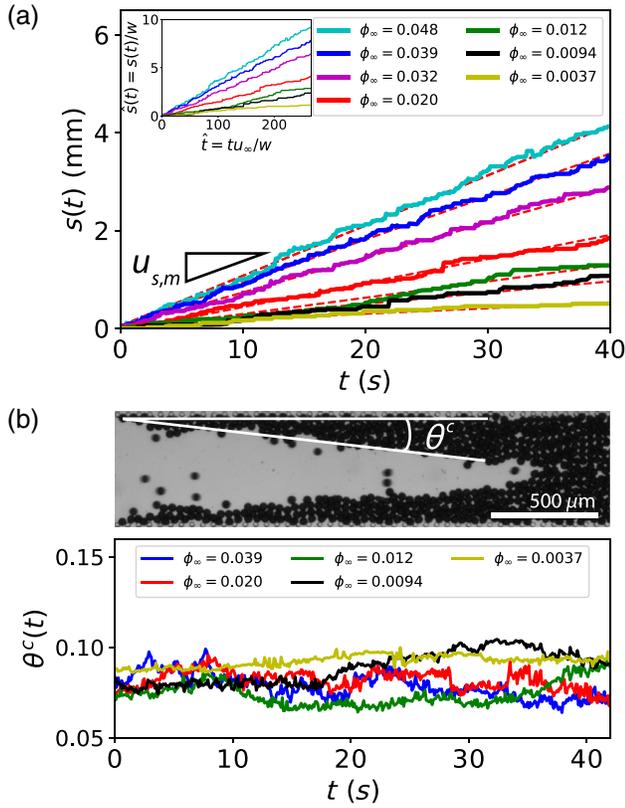
FIG. 2. (a) $s(t)$ taken at constant pressure for different incident volume fractions, ϕ_∞. The clog speed, $u_{s,m}$, is the derivative of $s(t)$. Inset: nondimensionalized clog position $\hat{s}(t) = s(t)/w$ plotted against nondimensionalized time $\hat{t} = tu_\infty/w$. (b) Top: micrograph of a clog with angle θ^c used to characterize shape indicated. Bottom: angle fluctuations (in radians) of the clog in time.

Once the clog shape reaches steady state, we can estimate the clog shape and angle using mass balance, noting that it is determined by fluid shunting through the leaky wall and along the gutter over a scale comparable to the width of the channel. The leaky wall and the gutter together form a pair of flow resistors in series; the larger of the two resistances controls the angle of the clog within which the fluid velocity is very small; see Fig. 3(b) for a schematic. To understand this qualitatively, we let X be the projected length of the clog along the x axis and $f \in [0, 1]$ the leakiness of the wall and the porosity of the bulk of the clog with $f \sim 0$ corresponding to the impermeable limit. Then the fluid flux through the wall over a scale comparable to half the width of the channel and along the length X must be equal to the added flux in the gutter through its width ℓ_g. Thus, $u_w w X f/2 \simeq u_g \ell_g X$, i.e., $u_g/u_w \sim wf/2\ell_g$. A simple geometric interpolant for the clog angle with the right limits is $\theta^c \sim \tan^{-1}(u_g/u_w) \sim \tan^{-1}(wf/2\ell_g)$; we leave a calculation for its exact form once the clog reaches steady state as an interesting follow-up.
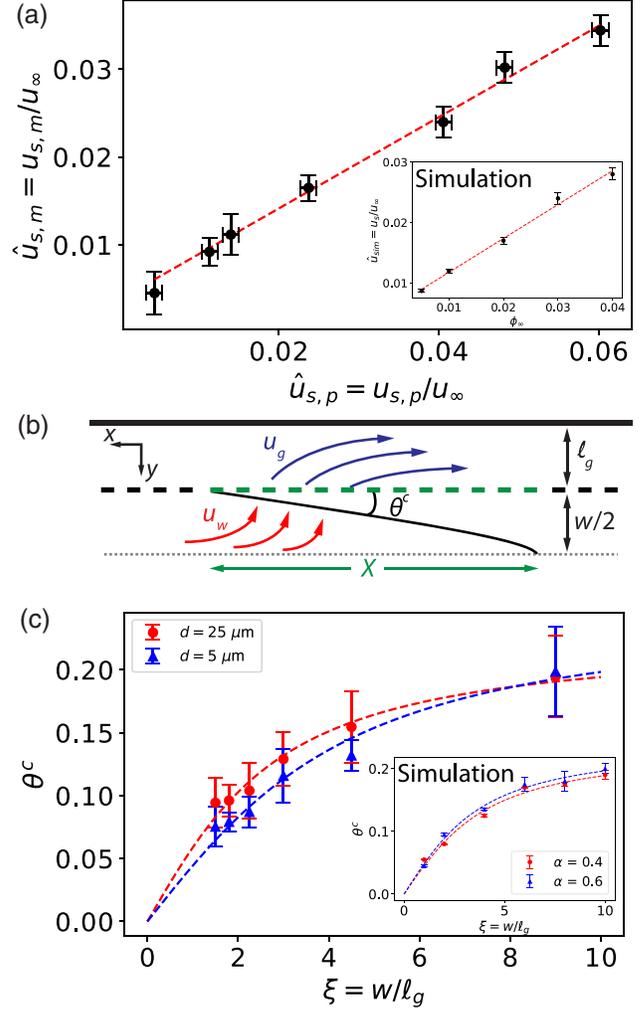

FIG. 3. (a) The ratio of the normalized measured clog speed, $\hat{u}_{s,m} = u_{s,m}/u_\infty$, plotted against the normalized predicted clog speed, $\hat{u}_{s,p} = u_{s,p}/u_\infty$. The red dashed line is a fit to data, $\hat{u}_{s,m} = 0.52\hat{u}_{s,p}$. Inset: simulated nondimensionalized clog speed, $\hat{u}_{\text{sim}} = u_s/u_\infty$, plotted against ϕ_∞. (b) Schematic of the half plane of a clog with stationary shape with labeled velocity and length scales. (c) Plot of θ^c (radians) versus $\xi = w/\ell_g$. Red circular points correspond to devices with $d = 5$ μm and blue triangular points to $d = 25$ μm. The red and blue dashed lines are fits to the data given, respectively, by $\theta^c = 0.14 \tan^{-1}(0.43\xi)$ and $\theta^c = 0.16 \tan^{-1}(0.28\xi)$. Inset: simulated clog angle plotted as a function of ξ with $\alpha = 0.4$ and 0.6.

To test this, we performed experiments where we held the pore spacing fixed at 5 and 25 μm and vary the gutter width between 50 μm $< \ell_g < 300$ μm in increments of 50 μm. In Fig. 3(c), θ^c is plotted as a function of the dimensionless ratio $\xi = w/\ell_g$. The red circular trace corresponds to devices with $d = 5$ μm and the blue triangular trace corresponds to devices with $d = 25$ μm. For both sets of devices, θ^c increases with ξ. When $\xi \simeq 9$ (at $\ell_g = 50$ μm), it becomes more difficult to distinguish devices with different pore spacings; the average angles are
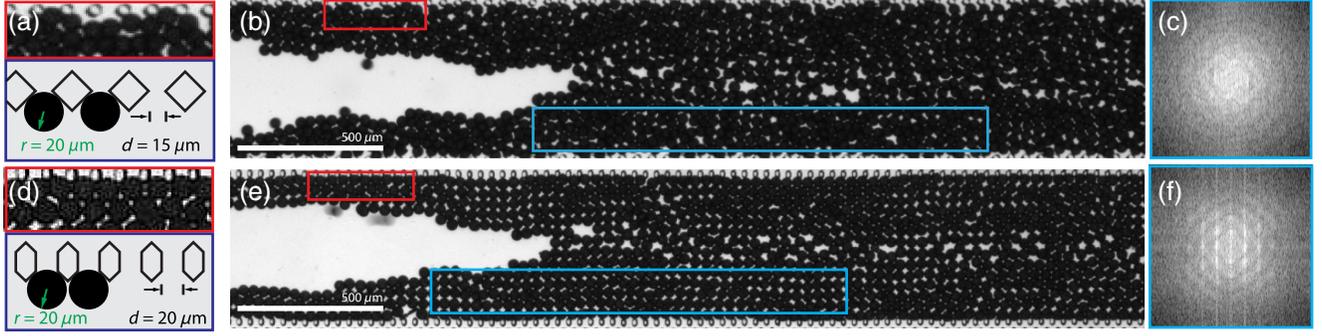
FIG. 4. (a) Top: optical micrograph of the particle packing near the top leaky membrane of a device with $d = 15$ μm. Bottom: schematic of the leaky membrane feature spacing and particle dimensions. (b) Snapshot of a particle clog in a device with $d = 15$ μm. (c) Two-dimensional fast Fourier transform of the area in the bottom rectangular box in (b). (d)–(f) Same as (a)–(c) but with $d = 20$ μm so that shunted particles close pack along the leaky wall.

fixed around $\theta^c \simeq 0.2$ rads. As ξ decreases the traces split, monotonically decrease, and begin to saturate to a final angle set by the pore spacing. The dashed lines in Fig. 3(c) are fits to $\theta^c = a\tan^{-1}(b\xi)$, where a and b are fitting parameters. As $\xi \rightarrow 0$, the dominant resistance in the system is from the leaky wall, so we expect the clog angle to saturate, leading to deviations from the simple prediction, observed in our experiments.

To understand these results in the asymptotic limits, we note that local pressure drop across the leaky wall, $\Delta P_w/d$, determines the fluid velocity through the wall via Darcy's law, $\Delta P_w/d \sim \mu u_w/d^2$, where μ is the fluid viscosity and u_w is the fluid velocity through the leaky wall. Here we have assumed that the width of the leaky wall is of order d. Similarly, fluid moving through the gutter is described by the relation $\Delta P_g/L \sim \mu u_g/\ell_g^2$ where $\Delta P_g/L$ is the pressure drop across the length of the gutter and u_g is the fluid velocity in the gutter so that the ratio of fluid resistances of the gutter to the leaky wall is given by $R = (\Delta P_g/L)/(\Delta P_w/d) \sim wfd^2/\ell_g^3$. We note that the limit as $\ell_g \rightarrow 0$, $R \rightarrow \infty$ corresponds to shrinking the gutter to zero width, while the limit as $f \rightarrow 0$, $R \rightarrow 0$ corresponds to decoupling the channel from the gutter; in either limit, the clog is vertical as expected, since the larger of the two resistances dominates.

To complement our experimental study and scaling analysis, we also perform numerical simulations of the leaky system within an Euler-Lagrangian (EL) framework. The EL framework models the carrier fluid as a continuum and evolves the particles in a Lagrangian manner based on spatiotemporally varying local hydrodynamic forces. For more detail on the numerical methods, see [27–29] and references therein. The carrier fluid motion is governed by the incompressible Navier-Stokes equations, and we use the immersed boundary method to impose the influence of the leaky wall on the carrier fluid governing equations. The colloidal particles first experience hydrodynamic drag from the carrier fluid and are then evolved according to a local Maxey-Riley dynamical equation, [30]. Forces from local shear in the fluid and rotation of the particles are negligible due to the low shear-rate and small particle size and are thus ignored in the particle evolution equation (see the Supplemental Material [25] for details). Varying the dimensionless ratio ξ and the permeability of the leaky wall allows us to compare the simulations with experiments. In the simulations, the leakiness of the wall is represented by the physical parameter $\alpha \in [0, 1]$ with $\alpha = 1$ corresponding to an impermeable wall with no-slip boundary conditions. The inset in Fig. 3(a) shows the scaled clog speed $\hat{u}_{sim} = u_s/u_\infty$ versus ϕ_∞ obtained from simulations, and captures the experimentally observed linear trend with the right prefactor. In the inset in Fig. 3(c), we plot θ_c versus $\xi = w/\ell_g$ for $\alpha = 0.4$ and 0.6 as computed from the numerical simulations. We observe good qualitative agreement with the experiments but note that there are some quantitative differences between the experimental measurements and numerical simulations due to coarse graining of the clogging front.

Finally, we turn to examine how the spatial order of particles in the bulk and on the boundary of the clog changes when we alter the geometry of the leaky wall. In Fig. 4(a), an optical micrograph of the top edge of a clog against a porous membrane with $d = 15$ μm is shown above a cartoon depiction. In these devices, the particles along the clog's perimeter are heterogeneously spaced, inducing disorder in the bulk of the clog as well. The 2D fast Fourier transform of the demarcated region of the bottom of the clog in Fig. 4(b), shown in Fig. 4(c), shows no discernable structure. When adjusting the wall geometry so that particles on the boundary of the clog form an ordered close-packed monolayer as seen in Fig. 4(d), incident particles stack layer-by-layer from the boundary into the bulk as the clog propagates backwards (see Supplemental Material [25], Video 4). Down the middle of the clog, where fluid is not shunted, there is a seam of disorder. The fast Fourier transform in Fig. 4(f) of the portion bound in Fig. 4(e) shows a structure corresponding to square packed particles.

Our variation of a microfluidic channel to include leaky walls and an adjoining gutter allows us to control the speed and shape of a jam when a suspension flows through it. Shunting of fluid through the leaky wall permits clogs to propagate backwards indefinitely with a constant speed and shape. Additionally, by structuring the leaky wall, we can control the ordering of particles in the clog. Together, our results might have implications for how physiology might already take advantage of leaky channels, and how one might engineer channels to achieve different types of nonequilibrium packings—but these are problems for the future.

[*]Lmahadev@g.harvard.edu

[1] J. Higgins, D. Eddington, S. Bhatia, and L. Mahadevan, Proc. Natl. Acad. Sci. U.S.A. **104,** 20496 (2007).

[2] K. Drescher, Y. Shen, B. L. Bassler, and H. A. Stone, Proc. Natl. Acad. Sci. U.S.A. **110,** 4345 (2013).

[3] P. Patil, T. Kumeria, D. Losic, M. Kurkuri et al., RSC Adv. **5,** 89745 (2015).

[4] E. Loiseau, G. Massiera, S. Mendez, P. A. Martinez, and M. Abkarian, Biophys. J. **108,** 2623 (2015).

[5] H. M. Wyss, D. L. Blair, J. F. Morris, H. A. Stone, and D. A. Weitz, Phys. Rev. E **74,** 061402 (2006).

[6] A. Sauret, E. C. Barney, A. Perro, E. Villermaux, H. A. Stone, and E. Dressaire, Appl. Phys. Lett. **105,** 074101 (2014).

[7] S. S. Massenburg, E. Amstad, and D. A. Weitz, Microfluid. Nanofluid. **20,** 94 (2016).

[8] A. Sauret, K. Somszor, E. Villermaux, and E. Dressaire, Phys. Rev. Fluids **3,** 104301 (2018).

[9] K. To, P.-Y. Lai, and H. Pak, Phys. Rev. Lett. **86,** 71 (2001).

[10] I. Zuriguel, L. A. Pugnaloni, A. Garcimartin, and D. Maza, Phys. Rev. E **68,** 030301 (2003).

[11] I. Zuriguel, A. Garcimartín, D. Maza, L. A. Pugnaloni, and J. Pastor, Phys. Rev. E **71,** 051303 (2005).

[12] C. Thomas and D. J. Durian, Phys. Rev. E **87,** 052201 (2013).

[13] J. Tang and R. P. Behringer, Europhys. Lett. **114,** 34002 (2016).

[14] X. Hong, M. Kohne, M. Morrell, H. Wang, and E. R. Weeks, Phys. Rev. E **96,** 062605 (2017).

[15] D. Helbing, I. Farkas, and T. Vicsek, Nature (London) **407,** 487 (2000).

[16] T. Nagatani, Rep. Prog. Phys. **65,** 1331 (2002).

[17] I. Zuriguel, D. R. Parisi, R. C. Hidalgo, C. Lozano, A. Janda, P. A. Gago, J. P. Peralta, L. M. Ferrer, L. A. Pugnaloni, E. Clément et al., Sci. Rep. **4,** 7324 (2015).

[18] E. Dressaire and A. Sauret, Soft Matter **13,** 37 (2017).

[19] A. S. Berman, J. Appl. Phys. **24,** 1232 (1953).

[20] S. Yuan, J. Appl. Phys. **27,** 267 (1956).

[21] G. Belfort, R. H. Davis, and A. L. Zydney, J. Membr. Sci. **96,** 1 (1994).

[22] D. C. Duffy, J. C. McDonald, O. J. Schueller, and G. M. Whitesides, Anal. Chem. **70,** 4974 (1998).

[23] J. C. Crocker and D. G. Grier, J. Colloid Interface Sci. **179,** 298 (1996).

[24] D. B. Allan, T. Caswell, N. C. Keim, and C. M. van der Wel, TRACKPY v0.4.1. https://doi.org/10.5281/zenodo.1226458 (2018).

[25] See the Supplemental Material at http://link.aps.org/supplemental/10.1103/PhysRevLett.125.044501 for data and discussion of clogging in channels with impermeable walls, data for $s(t)$ for leaky channels over hundreds of seconds, descriptions and videos of the experiments, description of the simulations, and videos of the simulations.

[26] W. Thielicke and E. Stamhuis, J. Open Res. Software **2,** e30 (2014).

[27] E. A. Fadlun, R. Verzicco, P. Orlandi, and J. Mohd-Yusof, J. Comput. Phys. **161,** 35 (2000).

[28] V. Spandan, V. Meschini, R. Ostilla-Mónico, D. Lohse, G. Querzoli, M. D. de Tullio, and R. Verzicco, J. Comput. Phys. **348,** 567 (2017).

[29] V. Spandan, D. Lohse, M. D. de Tullio, and R. Verzicco, J. Comput. Phys. **375,** 228 (2018).

[30] M. R. Maxey and J. J. Riley, Phys. Fluids **26,** 883 (1983).